(Preprint) AAS 14-094

DEFINITION OF THE DESIGN TRAJECTORY AND ENTRY FLIGHT CORRIDOR FOR THE NASA ORION EXPLORATION MISSION 1 ENTRY TRAJECTORY USING AN INTEGRATED APPROACH AND OPTIMIZATION

Luke W. McNamara[*], Robert D. Braun[†]

One of the key design objectives of NASA's Orion Exploration Mission 1 (EM-1) is to execute a guided entry trajectory demonstrating GN&C capability. The focus of this paper is defining the flyable entry corridor for EM-1 taking into account multiple subsystem constraints such as complex aerothermal heating constraints, aerothermal heating objectives, landing accuracy constraints, structural load limits, Human-System-Integration-Requirements, Service Module debris disposal limits and other flight test objectives. During the EM-1 Design Analysis Cycle 1 design challenges came up that made defining the flyable entry corridor for the EM-1 mission critical to mission success. This document details the optimization techniques that were explored to use with the 6-DOF ANTARES simulation to assist in defining the design entry interface state and entry corridor with respect to key flight test constraints and objectives.

INTRODUCTION

The NASA Orion Exploration Mission 1 (EM-1) is scheduled to be launched as early as 2017 from the Kennedy Space Center. This is scheduled to be the next Orion flight following the completion of Orion Exploration Flight Test 1[2] . This uncrewed EM-1 mission will provide a critical step forward in preparing Orion for future missions. The Orion spacecraft, assembled with a Service Module provided by the European Space Agency, is scheduled to be launched using the newly designed NASA Space Launch System (SLS). After a successful EM-1, EM-2 will become the first crewed mission to use the Orion spacecraft and SLS.

The EM-1 mission will be a mission 25 day mission to a Distant Retrograde Orbit (DRO) and will spend approximately 5 days in the DRO. After the DRO the spacecraft will return to Earth and reenter the atmosphere at approximately 11 $\frac{km}{sec}$ (36,090 $\frac{ft}{sec}$). Once inside the atmosphere, the vehicle will fly a guided entry using Guidance, Navigation, and Control (GN&C) bank angle modulation. The vehicle will target a splashdown location in the Pacific Ocean west of San Diego, CA.

The GN&C system works to enable the completion of several mission objectives. The navigation subsystem provides the guidance subsystem with deduced acceleration, velocity, and position in translation and rotation. The guidance subsystem uses that information to target the desired landing site using the guidance algorithm PredGuid[8,9,10,11] . PredGuid pairs a modern Numeric Predictor

[*]Aerospace Engineer, Flight Mechanics & Trajectory Design Branch, NASA Johnson Space Center, Houston, Texas, 77058, USA, luke.w.mcnamara@nasa.gov.

[†]Professor, Daniel Guggenheim School of Aerospace Engineering, Georgia Institute of Technology, Atlanta, Georgia, 30332, USA.

Corrector (NPC) with the flight-tested Apollo Final Phase guidance algorithm.[12] This combination is designed to perform the skip-entry at Earth which enables the vehicle to reach the target landing site from greater ranges. To reach the target landing location the guidance algorithm calculates the necessary bank angle to decrease the expected error in touchdown range-to-target throughout the flight.

Entry Sequence

The entry sequence will begin at the separation of the Crew Module (CM) from the Service Module (SM) prior to the Entry Interface (EI). The geodetic altitude of EI where the atmospheric density of Earth begins to have an impact on the trajectory is 121,920 m (400,000 ft). Between CM-SM separation and EI the vehicle is rotated heat shield forward to prepare for entry. During the hypersonic, supersonic, and subsonic portion of the trajectory before the Landing Recovery (LRS) sequence is initiated, the vehicle is banked by guidance pointing the vehicle lift vector in order to target the landing site. During the LRS sequence, as currently planned, the Crew Module will deploy Forward Bay Cover (FBC) pilot parachutes pulling away the FBC, deploy two drogue parachutes, release the drogue parachutes, and deploy three pilot parachutes which pull out the three main parachutes. The described parachute sequence for the EM-1 Entry, Descent & Landing (EDL) flight is illustrated in Figure 1 below.

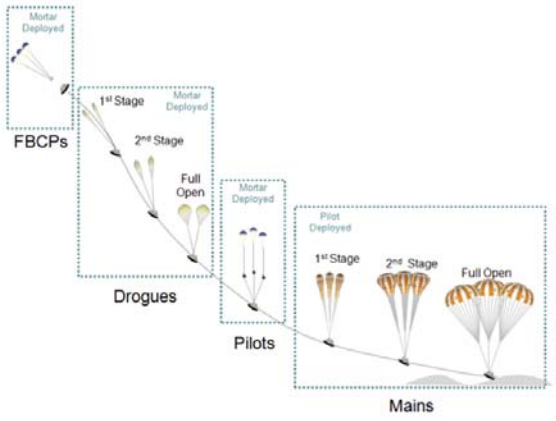

Figure 1. Orion EM1: Nominal Parachute Sequence[15]

Trajectory Generation

Trajectoies were generated with Advanced NASA Technology Architecture for Exploration Studies (ANTARES)[7], a six degree-of-freedom simulation, that numerically propagates the state vectors of the simulation bodies forward in time. ANTARES was configured to use prototype flight software rather than Rapid Algorithm MATLAB/Simulink® Engineering Simulation (RAMSES) flight software to increase flexibility and decrease required Computer Processing Unit (CPU) run time. The PredGuid guidance algorithm that was employed uses a numerical predictor-corrector combined with the Apollo Final Phase Entry Guidance. The PredGuid guidance gain set and reference trajectories were retuned or at least recalculated for varying $\frac{L}{D}$ and entry range to keep the expected trajectory performance including uncertainties inside the energy bucket described by Bairstow.[10] To analyze the impacts of uncertainties in the design process, Monte Carlo (MC) analyses are used

to model the uncertainties as random dispersions on the simulation models and inputs. For example Monte Carlo dispersions are applied to the aerodynamic characteristics, initial position vector and velocity vector, initial body attitude and rates, atmospheric characteristics, monthly atmosphere, initial navigation errors, Global Position System (GPS) errors, Inertial Measurement Unit (IMU) errors, aerodynamic Reaction Control System (RCS) jet interactions, RCS jet thrusts and specific impulses *etc*.

The EI position and velocity are dispersed using a 6x6 state covariance in the UVW frame also called the RSW frame.[16] The expected state covariance is progressively being refined with more analysis and testing. The atmospheric dispersions are dispersed using the Global Reference Atmosphere Model (GRAM) 2010 version 3.0.[13]

ANTARES was configured to simulate the trajectories using the physics models given in Table 1 and GN&C models in Table 2 among others.

Table 1. Physics Models

Physics	Computer Model
Atmosphere	GRAM 2010 V3.0[13]
Aerodynamics	MPCV Aerodynamic Database V0.71.1[14,3]
Aerothermal Dynamics	MPCV Aerothermal Database V0.93
Gravitation	NASA's JEOD Version 1.5.2

Table 2. GN&C Models

GN&C Component	Computer Model
Guidance	PredGuid C-Code Flight Software
Navigation	Discreet Extended Kalman Filter using GPS, Barometric Altimeter, IMUs
Control	Proportional-Derivative Control using RCS

ENTRY FLIGHT CORRIDOR DESIGN

The capability of an entry vehicle to accomplish its objectives and meet its multitude of constraints is a challenge. Typically constraints from other subsystems bound available domain space in most or all directions.

Problem Description

The purpose of defining the flight corridor is to capture and integrate constraints to understand the flyable domain of the vehicle. Once the constraints are integrated the corridor needs to protect for dispersions and facilitate design sensitivities[1,4]. The current objective is to minimize CM mass at touchdown. To meet this many options are possible but the hope is to not increase operational complexity to accomplish it. As such, the GN&C objective is to find a suitable minimum value of lift-over-drag, $\frac{L}{D}$*, to reduce the amount of ballast mass needed to position the center-of-gravity (CG)[6] accordingly. To achieve an increased $\frac{L}{D}$ value requires an increase in the required ballast mass. The $\frac{L}{D}$ is adequate if the design satisfies all the probabilistic constraints for predicted uncertainties modeled using Monte Carlo simulations. Such uncertainties are on atmospheric properties,

*For the meanings of variables refer to the Notation section near the end of the document.

initial position, initial velocity, reaction control system effective thrust, aerodynamics *etc*. A secondary goal is to gain insight into the sensitivity impacts of independent variables and dependent variables on the integrated corridor.

Hence, find the solution $\frac{L}{D}_{min}$ which minimizes the performance index F($\vec{x}$) in Equation 1 where $\vec{x}$ is given in Equation 2, the available corridor width, $c(\vec{x})$, is given in Equation 3 and the requirement for protected corridor width, z, currently equals 0.15 degrees (previously was 0.30 degrees).

$$F(\vec{x}) = c - z \tag{1}$$

$$\vec{x} = \left[\begin{array}{cccccc} V_{EI} & \gamma_{EI} & \psi_{EI} & \lambda_{EI} & \delta_{EI} & m_{EI} \end{array} \quad \frac{L}{D}_{Mach=25} \right]^T \tag{2}$$

$$c(\vec{x}) = \gamma_{EI,shallow\,limit} - \gamma_{EI,steep\,limit} \tag{3}$$

As the combined aerothermal and TPS structures groups desire to save TPS mass, and findings have indicated the result that this occurs at shallower flight-path-angles the objective from this group is γ_{max} of an available corridor. As such, that secondary objective is treated after finding the $\frac{L}{D}_{min}$ from the GN&C design corridor.

To define the design cycle for an entry corridor is subjective given the multiple independent variables. The technique employed here uses the following path of steps but there are many other paths that would lead to the same conclusion.

First, define the mission goal to be to return from a specific orbital body or point in space defined for EM-1. That defines the EI state return velocity range. Then use the *minimum* acceptable downrange to satisfy the crew HSIR, disposal concerns *etc*. Typically the minimum downrange case is defined to provide divert capability to avoid a large disruptive weather system such as a hurricane in the Pacific Ocean. Then follow the design cycle illustrated in Figure 2 below to converge on an acceptable corridor.

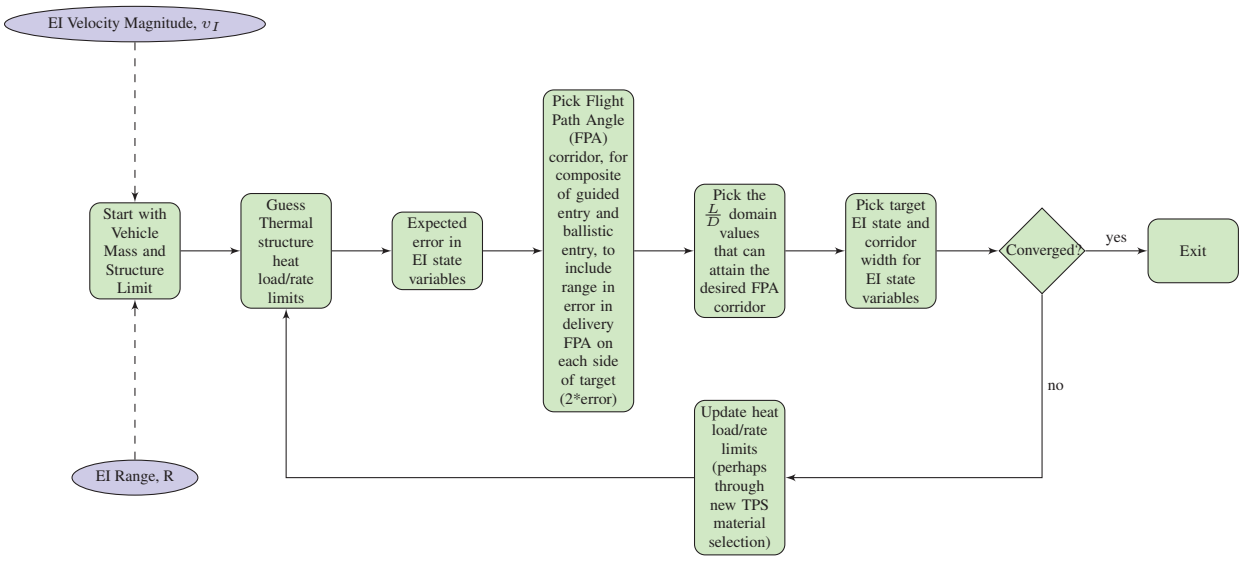

Figure 2. One Version of a Design Cycle for Entry Corridor

If after the last step in Figure 2 the solution has been identified (converged) the process is complete. If not, then pick new heat load/rate limits and repeat steps 2 through 6. Then repeat the process for the *longest* beneficial downrange case. Due to the geometry of the Earth this range is 8890 km (4800 n.mi) to have the ability to return to the desired landing site (based on its latitude) at any time during the lunar month.

The key design constraints of the EM-1 entry trajectory corridor design are listed below with their probability success criteria.

1. **Guided Vehicle Landing Accuracy.** The landing accuracy requirement is for the vehicle to land within 10 km (5.4 nautical miles [n.mi.]) of the desired landing site with a probability of success of 99.865% (3σ) at 90% confidence. As this requirement is treated in two pieces, a steep piece and a shallow piece, this is treated as two separate single tail distributions. Thus, this probability equates to allowing 1 miss for a 3000 case Monte Carlo analysis.

2. **Service Module Debris.** The SM debris requirement is for potential SM debris to land outside of buffer zones around foreign and domestic landmass with a probability of success of 99.865% (3σ) at 95% confidence. This probability equates roughly to allowing 0 failures for a 3000 case Monte Carlo analysis. This requirement is based on NASA Technical Standard (NASA-STD 8719.14), an accompaniment to the NPR for Limiting Orbital Debris (NPR 8715.6A), and is designed to limit the risk of human casualty due to end of mission disposal of jettisoned items.

3. **Guidance Degradation.** It is desired that the entry guidance not succumb to atmospheric gradients that yield degraded performance. This protection ensures that guidance is able to protect against cases with HSIR violations between EI and drogue parachute deployment.

4. **Guided Human System Integration Requirements (HSIR).** The subset of Human System Integration Requirements (HSIR) this is concerned with are a set of requirements on the sustained crew member sensed linear acceleration, rotational acceleration, coupled rotational acceleration, rotational velocity and linear jerk. The requirement is to be satisfied for a probability of success of 99.865% (3σ) at 99% confidence which equates roughly to 0 failures in a 3409 case sample size Monte Carlo.

5. **Ballistic Human System Integration Requirements (HSIR).** The subset of Human System Integration Requirements (HSIR) this is concerned with are a set of requirements on the sustained crew member sensed linear acceleration, rotational acceleration, coupled rotational acceleration, rotational velocity and linear jerk. For the back-up mode of ballistic entry, executed in case of certain failures, the sensed linear acceleration limits are relaxed from the nominal guided entry case. The requirement is to be satisfied for a probability of success of 99.865% (3σ) at 99% confidence which equates roughly to 0 failures in a 3409 case sample size Monte Carlo.

6. **Ballistic Entry Altitude Rate.** The geodetic altitude rate is required to be less than or equal to zero to ensure successful atmospheric capture with a probability of success of 97.725% (2σ) at 90% confidence which equates roughly to 57 failures in a 3000 case sample size Monte Carlo.

7. **Ballistic Entry Structural Acceleration Load.** The Crew Module's structural acceleration load is required to be less than or equal to 15 g's. The requirement is to be satisfied for

a probability of success of 97.725% (2σ) at 90% confidence, which equates roughly to 57 failures in a 3000 case sample size Monte Carlo.

8. **Aerothermal Thermal Protection System (TPS) Backshell Panel Maximum Temperature.** This aerothermal TPS requirement is currently booked at constraining the trajectory to a value less than or equal to 3150 °F.

Listing all of these constraints in one equation yields

$$\vec{g} = \begin{bmatrix} g_1 \\ g_2 \\ g_3 \\ g_4 \\ g_5 \\ g_6 \\ g_7 \\ g_8 \\ g_9 \end{bmatrix} : \begin{bmatrix} \text{Guided Landing Accuracy} \leq 10 \text{ km (Steep Side)} \\ \text{Guided Landing Accuracy} \leq 10 \text{ km (Shallow Side)} \\ \text{Service Module Debris Disposal Limit} \\ \text{Ballistic HSIR} \\ \text{Ballistic Geodetic Altitude Rate} \leq 0 \\ \text{Guidance Degradation} \\ \text{Guided HSIR} \\ \text{Ballistic Structure Acceleration} \leq 15 \text{ g's} \\ \text{Aerothermal Backtile Temperature} \leq 3150 \text{ °F} \end{bmatrix} \tag{4}$$

Problem Solution Subspaces. After multiple corridor design cycles, due to system level constraints, the subspace of permissible independent variable combinations are defined as shown in Table 3 below.

Table 3. Down Selected Design Space as a Result of Mass Reduction Activities

Independent Variable	Minimum	Maximum
$\frac{L}{D}$ (nd)	0.23	0.27
EI velocity, v_I, ($\frac{m}{s}$)	10,950	11,050
CM Mass, m, (kg)	9,934 (21,900 lbm)	10,387 (22,900 lbm)
Downrange, R, (km)	2,408 (1,300 n.mi.)	6,482 (3,500 n.mi.)
Flight Path Angle Corridor Width, c, (degree)	0.15	0.15

DETERMINING CONSTRAINT CURVES

In order to assess the safe flyable corridor of the subspace the constraints need to be defined numerically using ANTARES simulations. As knowledge of the constraint curves are critical in assessing the flyable corridor the curves would ideally be identified to a high degree of precision. This interest in increasing the curve fit of constraint lines needs to be balanced against the associated computational demands and wait time. The computational demands are not limited to CPU run time but rather also include disk memory to store the necessary data.

The dependent variable constraint curve is defined by the associated independent variable set defined in Equation 2. Equation 2 can be rewritten into Equation 5 where range, R, has replaced longitude, λ, and δ has been removed (by tying the database to a fixed landing site).

$$\vec{x}_{independent} = \begin{bmatrix} V_{EI} & \gamma_{EI} & \psi_{EI} & R_{EI} & m_{EI} & \frac{L}{D}_{Mach=25} \end{bmatrix}^T \tag{5}$$

Hence for a given $\vec{x}_{independent}$ the dependent variable constraint curve could be characterized in all directions of the design space. To do that requires discretizing all dimensions of the $\vec{x}_{independent}$,

simulating a trajectory from each element of the discretized set in time from EI to touchdown, and processing all of the dependent variable data to identify each constraint curve. To plot the constraint curve in a figure showing more dimensions than two is problematic for ease of understanding. As such the curve can be shown in any two dimensional domain such as $\frac{L}{D}_{Mach=25}$ vs. γ_{EI}, V_{EI} vs. γ_{EI}, or $\frac{L}{D}_{Mach=25}$ vs. R_{EI}. As the intent is to locate the $\frac{L}{D}_{min}$ that provides a γ_{EI} corridor width of 0.15 degrees it makes the most sense for this case to use the $\frac{L}{D}_{Mach=25}$ vs. γ_{EI} domain to visualize the corridor.

Hence for a certain set of mission re-entry constants

$$\vec{x}_{constant} = \begin{bmatrix} V_{EI} & \psi_{EI} & R_{EI} & m_{EI} \end{bmatrix}^T \tag{6}$$

the entry corridor can be defined and visualized with respect to the independent variables

$$\vec{x}_{independent} = \begin{bmatrix} \gamma_{EI} & \frac{L}{D}_{Mach=25} \end{bmatrix}^T \tag{7}$$

and all the dependent variables can be found that define the constraints on the entry corridor in that two dimensional space.

There are only two parts to constraint curve fitting to be concerned with here, finding (γ, $\frac{L}{D}$) points on the curve, and deciding the order of the polynomial to fit to the curve. Ideally those points on the curve would be from individual dispersed Monte Carlo sets and there would be a sufficient amount to characterize the curve in all directions of the design space. Currently that is unrealistic given the computation capabilities of the team and also it would be unnecessary considering the nature of the inputs to the problem from multiple subsystems. It is realistic however to characterize a curve in two dimensions, γ and $\frac{L}{D}$, either using undispersed trajectories for speed and breadth or using dispersed Monte Carlo trajectory sets for statistical accuracy. Several methods are described below that use variations of these methods. In addition, to find the points on the curve there are two sets of techniques, namely grid search using brute force predetermined constant increment parametric sweeps or iteratively using an optimization scheme. Although due to the discontinuities of the dependent variables and trip points, finding points iteratively using an optimization scheme presents certain pitfalls.

Database of Undispersed Trajectories. A database of undispersed trajectories was generated for a discretized space of the same order as the number of independent variables in Equation 5, namely 7.

$$\vec{x}_{independent,discretized} = \begin{bmatrix} V_{EI} \epsilon \mathbb{R} | \{V_{min} \leq V \leq V_{max}\} \\ \gamma_{EI} \epsilon \mathbb{R} | \{\gamma_{min} \leq \gamma \leq \gamma_{max}\} \\ \psi_{EI} \epsilon \mathbb{R} | \{\psi_{min} \leq \psi \leq \psi_{max}\} \\ r_{EI} \epsilon \mathbb{R} | \{r_{min} \leq r \leq r_{max}\} \\ R_{EI} \epsilon \mathbb{R} | \{R_{min} \leq R \leq R_{max}\} \\ m_{EI} \epsilon \mathbb{R} | \{m_{min} \leq m \leq m_{max}\} \\ \frac{L}{D}_{Mach=25} \epsilon \mathbb{R} | \{\frac{L}{D}_{min} \leq \frac{L}{D} \leq \frac{L}{D}_{max}\} \end{bmatrix} \tag{8}$$

Here the $\vec{x}_{i,min}$ and $\vec{x}_{i,max}$ are defined wide enough to encapsulate any potential designs using input from orbit phase trajectory designers and the mass properties team. As such, for each element of the $\vec{x}_{independent,discretized}$ set a multitude of dependent variables is available to extract constraint

lines. This database is used to create undispersed corridors and perform sensitivities to all the independent variables quickly.

From Database of Undispersed Trajectories to Requirement Verification of Dispersed Trajectories.

Now as the design requirements are based on certain probability of success and confidence values including uncertainties, which are accounted for in trajectory design using dispersions on the trajectory models, an entry corridor would be more suitable by including the dependent variables (results) of the dispersed trajectories.

To do this the corridor lines need to be redrawn through the targeted $\vec{x}_{constant}$ that resulted in just meeting the requirement. The way this is done is using Monte Carlo. From binomial statistics the required probability of success and confidence level (value) are used to determine the necessary Monte Carlo sample size and number of cases from that sample size that are allowed to fail (not pass) the success metric.

Using Monte Carlo Anchor Points

Monte Carlo points identifying the constraint in the (γ, $\frac{L}{D}$) space are necessary to anchor the points with statistical meaning. Those points are found using an iterative method or with a grid searching method. In either case the constraint line is identified by analyzing adjacent sets of Monte Carlo's and finding the tripping point where the dependent variable begins to surpass the constraint. In the iterative method an automatic setup using a simple optimizer such as a line search can run a Monte Carlo, assess all of the dependent variables to determine if the augmented root (constraint value) had been found and repeat until a constraint point (γ, $\frac{L}{D}$) had been identified. This process means iterating with values of γ for a set constant $\frac{L}{D}$, for every $\frac{L}{D}$ anchor point needed, and repeating this process for every constraint. The convergence limit on the γ iterations can be set according to a fidelity γ tolerance such as 0.01 degrees. In the grid searching method for each (γ, $\frac{L}{D}$) anchor point needed per constraint, one fine parametric sweep of γ is performed for a set constant $\frac{L}{D}$. That sweep is then used to evaluate all of the constraints at that $\frac{L}{D}$.

A method to provide a good starting guess method for an iterative method,which has yet to be implemented, would be to use an iterative search method to locate a larger number of (γ, $\frac{L}{D}$) points. This method would start at a boundary point of the domain with an initial guess for a point on the curve, determined either by experience or from the undispersed database, and perform a 1-D line search to locate an initial point on the constraint. Then to find a subsequent point it would use a preset step size to traverse across the domain from one direction to the other based on the expected general orientation of the constraint in the domain (e.g. vertical, horizontal etc.). If the dependent data the line search is evaluating is continuous it may use gradient methods or even second gradient methods, while if it has discontinuities it will have to use zero-th order solvers such as the bisection method. After stepping in the expected direction of the constraint the routine would perform another 1-D line search to locate the (γ, $\frac{L}{D}$) on the constraint. Then the actual direction between the previous two points would be used as the step direction for the following step forward which would be followed by another 1-D line search. Storing the history of previous solutions should provide good initial guesses at each iteration step as most constraints can be closely modeled by low order polynomials. Essentially this is a method to walk along the constraint curve through the domain in order to characterize it.

Computational Demands The computational demands are a function of the number of Monte Carlo anchor points, the number of Monte Carlo sets needed to identify all of the constraints, the number of constraints, the number of CPUs, and the required CPU time per Monte Carlo set. With respect to the grid search method, the iterative method may require a decreased number of Monte Carlo sets to find a single constraint, but may require an increase in the total number of of Monte Carlos to find all of the constraints when summed together.

For the iterative method the total time would equate to that shown in Equation 9, assuming that the number of Monte Carlo iterations required to locate a constraint point is constant for each constraint.

$$\text{Time}_{\text{iterative method}} = \text{MC Anchor Points} \cdot \frac{\text{CPU time}}{\text{MC}} \cdot \frac{\text{MC iterations}}{g_i} \cdot dim(\vec{g}) \cdot \frac{1}{\text{No. CPUs}} \tag{9}$$

For the grid searching method the total time would equate to that shown in Equation 10.

$$\text{Time}_{\text{grid method}} = \text{MC Anchor Points} \cdot \frac{\text{CPU time}}{\text{MC}} \cdot \text{MC sweep of } \gamma \text{ values} \cdot \frac{1}{\text{No. CPUs}} \tag{10}$$

Clearly from comparing Equation 9 and Equation 10 the condition where the run time crosses over would be that shown in Equation 11.

$$\frac{\text{MC iterations}}{g_i} \cdot dim(\vec{g}) = \text{Number of Monte Carlos in sweep of } \gamma \text{ values} \tag{11}$$

So if the iterative method converges on each of the constraints quickly, and the number of constraints is small, it will reach a solution more quickly than the grid search method. The downfall of this method is that it requires a optimization routine, generates data that is not incremented spatially evenly, and does not provide insight into the sensitivity around each constraint limit in the domain space.

Table 4 presents approaches to constraint curve fitting that offer combinations of point finding techniques, number of anchor points, and the order of the polynomial curve fit to apply. The *beta* entry in the first row of Table 4 represents using the already constructed undispersed database. In Table 4 four of the listed methods use the polynomial curve fit assessed in the undispersed database and anchors it to one Monte Carlo constraint point in (γ, $\frac{L}{D}$) by translating it on the γ axis, namely methods 1, 5, 6, and 10. As such the constraint curve is really a pseudo-dispersed curve combining the speed and availability of the pre-existing undispersed database and the statistical accuracy of one Monte Carlo anchor point.

For EM-1 the entry corridor is often designed using the grid search approach labeled Method 7 in Table 4 with two high fidelity sweeps of γ gathering enough information to characterize two points of each of the constraints. That is enough to fit a linear line. Suppose the needed number of Monte Carlo anchor points is two, the required number of runs per Monte Carlo is approximately 3400, the time per run is approximately 30 seconds, the number of CPUs available is approximately 90, and the number of Monte Carlos in γ grid search is 200. The total time expectation for this process using Equation 10 is approximately 125 hours. On the other hand, cutting the needed number of Monte Carlo anchor points down to one, as suggested by Method 6 in Table 4 cuts the total time needed in half to roughly 62 hours. In that case the polynomial fit curve can be taken from the undispersed database and anchored (translated) by the determined anchor point. As yet, the idea of using more than two Monte Carlo anchor points, as in Method 8 and 9, has not been incorporated

Table 4. Constraint Curve Fitting Methods

Method	Point Finding Technique	Anchor Points Source	Number of Anchor Points	Polynomial Curve Fit Source	Polynomial Curve Fit Order
Beta	None	Undispersed	Database Specific	Preset by User	g_i Specific
1	Iteratively	Dispersed MCs	1	Undispersed Database	g_i Specific
2	Iteratively	Dispersed MCs	2	Preset by User	1
3	Iteratively	Dispersed MCs	3	Preset by User	2
4	Iteratively	Dispersed MCs	4	Preset by User	3
5	Iteratively	Dispersed MCs	Constraining 1 of n	Undispersed Database	g_i Specific
6	Grid Search	Dispersed MCs	1	Undispersed Database	g_i Specific
7	Grid Search	Dispersed MCs	2	Preset by User	1
8	Grid Search	Dispersed MCs	3	Preset by User	2
9	Grid Search	Dispersed MCs	4	Preset by User	3
10	Grid Search	Dispersed MCs	Constraining 1 of n	Undispersed Database	g_i Specific

due to their computational demands but that is planned for future work. For comparison consider if Method 1 was used which is the same as Method 6 except for using an iterative approach to finding anchor points. In that case, assuming there are 9 constraints and each constraint took consistently 10 iterations apiece then the total time would be roughly 28 hours.

The accuracy of the polynomial curve fits of the constraint curves, using the undispersed database, have been analyzed. The curves all appear to be modeled very well by polynomials of order 4 or 3, effectively by order 2, and in the case of certain constraints even effectively by order 2 or 1. Polynomial approximations of constraints using order 5 and even some using order 4 suggested statistical over-fitting issues. The Table 5 shows a few example constraints with the deduced best order for a polynomial fit, along with the associated sum of Root-Mean-Square (RMS) to indicate the accuracy of the fits.

Table 5. Constraint Curve Fitting: Guided, v_I=11.2, R=8890km (4800 n.mi)

Constraint	Side	Polynomial Order	Sum of RMS
Guided Landing Accuracy	Steep Side	4	0.0091057
Aerothermal TPS Backshell Panel Temperature	Top Side	4	0.0042080
HSIR (e.g. Crew sensed acceleration)	Steep Side	3	0.0064415

As this mission is still early on in the design process, before the Preliminary Design Review (PDR), the trajectory design is still being evolved cyclically with feedback from other subsystems such as aerothermal, TPS and structures. The GN&C team provides the aerothermal team with sufficient trajectory data for it to assess the aerothermal flight conditions. Then it typically verifies that the aerothermal dependent variables being used to assess aerothermal requirements are accurate and sufficient from which to make vehicle level trades. Then if the designed Monte Carlo trajectory sets exceed the aerothermal teams limits the integration community must decide to either change the trajectory, change the aerothermal modeling approach, or to change the vehicle hardware such as the TPS, gap fillers, outer mold line.

After the previous cycle the aerothermal team determined the following set to determine TPS sizing drivers. In previous design cycles GN&C has delivered trajectory data to the aerothermal team to assess for a large Monte Carlo run matrix composed of TPS size driving combinations of the following: $\gamma_{EI,shallow\,limit}$ or $\gamma_{EI,steep\,limit}$, guidance mode, EI inertial velocity magnitude, EI

range, $\frac{L}{D}$, γ_{EI}, and landing site. That cycle identified a sensitivity to γ_{EI} that is driving the TPS sizing with decreasing γ_{EI} (steepening) leading to increasing TPS mass, and conversely increasing γ_{EI} (shallowing) leading to decreasing TPS mass.

ENTRY CORRIDORS

After a recent cycle of creating and evaluating integrated entry corridors certain system level assumptions were made to permit decrease $\frac{L}{D}_{min}$ values and increase γ_{min} to decrease mass required for CG ballast placement and TPS sizing. In Figure 3 two pairs of entry corridors $\frac{L}{D}_{Mach=25}$ vs. γ_{EI} are shown for two different entry ranges that are 4630 km and 8890 km.

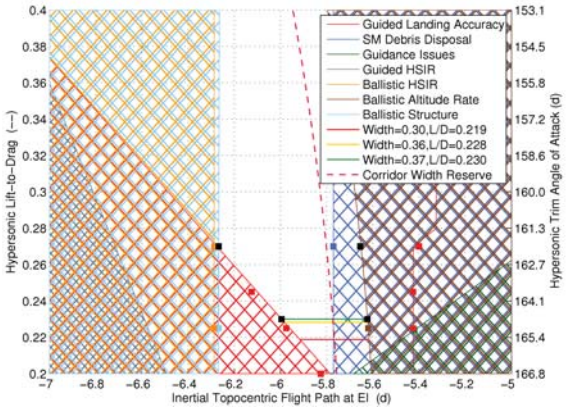

(a) Entry Corridor for Guided, v_I=10.95 $\frac{km}{s}$, R=4630 km (2500 n.mi.), Neglecting SM Debris Disposal Constraint

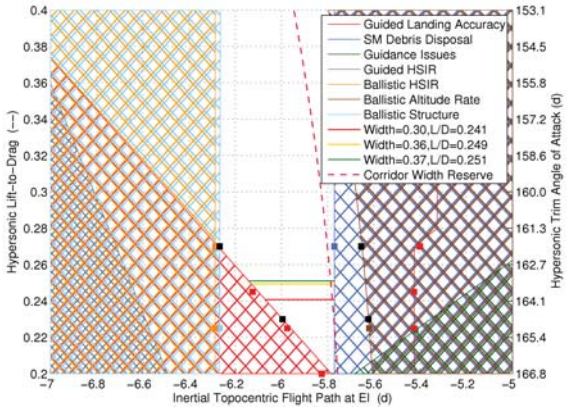

(b) Entry Corridor for Guided, v_I=10.95 $\frac{km}{s}$, R=4630 km (2500 n.mi.)

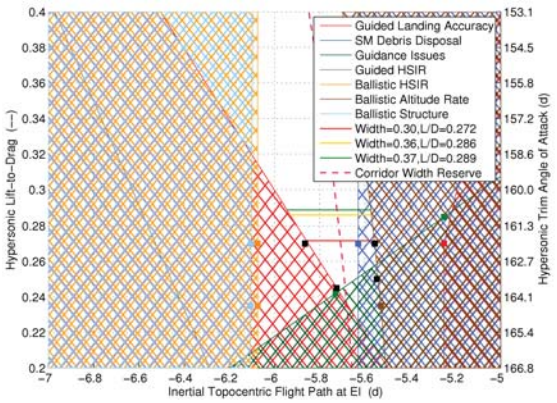

(c) Entry Corridor for Guided, v_I=10.95 $\frac{km}{s}$, R=8890 km (4800 n.mi.), Neglecting SM Debris Disposal Constraint

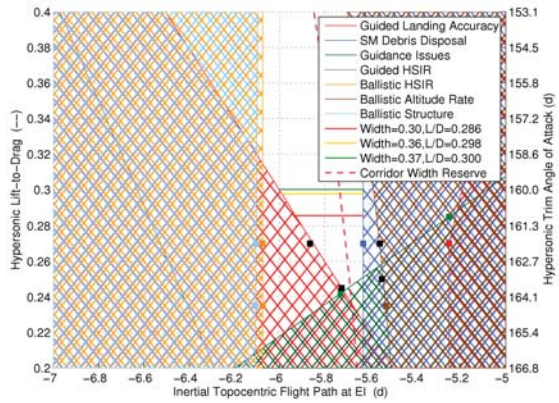

(d) Entry Corridor for Guided, v_I=10.95 $\frac{km}{s}$, R=8890 km (4800 n.mi.)

Figure 3. Entry Corridors

In the plots in Figure 3 the constraints have been represented by areas of color compressing the flyable corridor colored white. The constraints are identified in the legend along with the calculated corridor widths at three $\frac{L}{D}$ values. After doing more in-depth analyses of the low $\frac{L}{D}$ values in Figure 3(a) and Figure 3(b) the decision was made to hold the minimum $\frac{L}{D}$ at 0.23 as indicated in Table 3. The program has decided to neglect the SM debris disposal limit as it impacts the corridor design. To assess the impacts of this choice see Figure 3. The SM debris disposal line is indicated by the

blue line. The margin that the program has chosen to cover for γ_{EI} corridor width of 0.15 degrees is indicated as an offset red dashed line from the purple line representing the Ballistic 2σ lofting constraint. Hence, when the red dashed line (the 0.15 degree margin) is steeper than the SM debris disposal constraint the margin is adequate, but when it is shallower than the SM debris disposal constraint line the margin is inadequate and the design needs to move to the real SM boundary. The Monte Carlo anchor points that were used to anchor the constraint polynomials from the undispersed database are shown as squares. The squares that are blackened indicate the four extreme cases in the corridor that GN&C assessed and delivered to other subsystems for further analysis. It is clear from each pair of figures, Figure 3(a) with Figure 3(b) and Figure 3(c) with Figure 3(d), above that the assumption to ignore the impacts of SM debris disposal is a serious risk. To deal with this risk EM-1 is planning to perform a CM raise maneuver that it was not planning to previously. The combined CM and SM vehicle will target a steeper than nominal γ_{EI}, separate from each other leaving the SM at that return γ_{EI}, and then the CM will use its RCS jets to burn to shallow up its own γ_{EI}. This maneuver will ensure that the SM is not a risk to the public and that the CM can target a shallower γ_{EI} than it otherwise would be able.

CONCLUSION

The characterization of a spacecraft's entry corridor is governed by coupled nonlinear differential equations, active control, and inputs from many other subsystems. The characterization is sensitive to changes from other sub-systems such as mass properties, propulsion, aerodynamics, TPS, structures, *etc.*. Depending on the magnitude and direction of the changes the associated spacecraft entry corridor will change in different ways. Reacting repetitively to new inputs has lead to a large amount of strategic automation leveraging pre-existing understanding to characterize corridors quicker and more definitively each iteration. This improvement has lead to the entry corridor being the one of the first steps in assessing a spacecraft's re-entry capabilities.

FUTURE WORK

The authors acknowledge this work is in support of a mission that has yet to reach Preliminary Design Review (PDR) and will surely make design changes in the coming design cycles that cannot be foreseen and taken into account. Thus this work will be continued in order to improve the robust capability and speed of evaluating re-entry flight corridors for vehicle design changes. It is the intent that as the design process advances other trajectory requirements will be taken in account in the entry corridor design including drogue parachute deployment flight condition, main parachute deployment flight condition, landing and touchdown heading angle among others.

ACKNOWLEDGMENT

This work was carried out by the NASA Johnson Space Center. The author would like to thank Jeremy R. Rea and Timothy J. Crull of NASA Johnson Space Center for trajectory products and inputs that aided this work. The author would also like to thank his family for their support.

NOTATION

c	Flight Path Angle Corridor Width
$\frac{L}{D}$	Lift-over-Drag Ratio at Mach Number of 25 of Vehicle
m	Vehicle Mass at Entry Interface
R	Downrange
v	Earth Centered Inertial Velocity Vector Magnitude of Vehicle
δ	Geodetic Latitude
γ	Inertial Topocentric Flight Path Angle
ψ	Inertial Topocentric Azimuth
λ	Longitude

REFERENCES

[1] McNamara, Luke W., "DAC3 Entry Corridor for Lunar and LEO Returns," Tech. Rep. FltDyn-CEV-09-84, NASA Johnson Space Center, Houston, TX, June 2009.

[2] McNamara, Luke W., "Entry Atmospheric Flight Control Authority Impacts on GN&C and Trajectory Performance for Orion Exploration Flight Test 1", AIAA Guidance, Navigation and Control Conference, AIAA Paper Number 2012-4994, Minneapolis, Minnesota, August 13-16 2012,.

[3] McNamara, Luke W., "Flight Dynamics/GN&C Assessment of MPCV Aerodynamic Database Version 0.71.1," Tech. Rep. FltDyn-CEV-12-85, NASA Johnson Space Center, Houston, TX, January 2013.

[4] Rea, Jeremy R., "Orion Entry Flight Corridor Analysis," AIAA Guidance, Navigation and Control Conference and Exhibit, No. 2008-7153, Honolulu, HI, August 2008.

[5] Rea, Jeremy R., "Entry Corridor Analysis Supporting Command Module Separation State Definition for Orion Flight Test 1 Periodic Technical Review 2," FltDyn-CEV-11-23, CEV Flight Dynamics Entry Team, NASA Johnson Space Center, Houston, TX, April 2011.

[6] Rea, Jeremy R., "Orion Entry Performance-Based Center-of-Gravity Box," AIAA Guidance, Navigation and Control Conference and Exhibit, No. 2010-8061 in AIAA, August 2010.

[7] Hoelscher, Brian R., "Orion Entry, Descent, & Landing Simulation," AIAA Guidance, Navigation and Control Conference and Exhibit, No. 2007-6428 in AIAA, August 2007.

[8] Putnam, Zachary R., Rea, Jeremy R., "A Comparison of Two Skip Entry Guidance Algorithms," AIAA-2007-6424, August 2007.

[9] Putnam, Zachary R., Neave M. D., Barton G. H., "PredGuid Entry Guidance for Orion Return from Low Earth Orbit," IEEE Aerospace Conference, No. 05447010, 2010.

[10] Bairstow, S. H., "Reentry Guidance with Extended Range Capability for Low L/D Spacecraft," S. M. Thesis, Department of Aeronautics and Astronautics, Massachusetts Institute of Technology, February 2006

[11] Bairstow, S. H, Barton, G., "Orion Reentry Guidance with Extended Range Capability Using PredGuid," AIAA-2007-6427, August 2007.

[12] Morth, R., "Reentry Guidance for Apollo," MIT/IL R-532 Vol. I, 1966.

[13] NASA TM-2011-216467, "The NASA MSFC Earth Global Reference Atmospheric Mode-2010 Version," C.G. Justus, F.W. Leslie, NASA Marshall Space Flight Center, AL, June 2011.

[14] NASA EG-CEV-06-37, "Formulation of the Orion MPCV Aerodynamic Database, Ver 0.71.1," MPCV Aerosciences Team, NASA Johnson Space Center, Houston, TX, December 2012.

[15] LM-ORN-0863, Revision 000, "Orion Exploration Mission Simulation Data Book," Lockheed Martin Space Systems Co., Denver, CO, June 14, 2013.

[16] Vallado, D. A, "Fundamentals of Astrodynamics and Applications", Third Edition, p.163-172, Springer, New York, 2007.